Int. J. Heat Mass Transfer. Vol. 35, No. 3, pp. 649–657, 1992
Printed in Great Britain

0017–9310/92 $5.00 + 0.00
Pergamon Press plc

Steady-state and transient temperature field in the absorber tube of a direct steam generating solar collector†

W. HEIDEMANN, K. SPINDLER and E. HAHNE
Institut für Thermodynamik und Wärmetechnik, Universität Stuttgart,
Pfaffenwaldring 6, D-7000 Stuttgart 80, F.R.G.

Abstract—The temperature field in the absorber tube of a direct steam generating parabolic trough collector is calculated. Steady-state and transient operating conditions are considered. A universal program was developed for solving the two-dimensional transient temperature field using a modular nodal point library. The temperature field is extremely asymmetric due to the variation of the heat transfer coefficient at the inner surface and the solar irradiation at the outer surface of the absorber tube. High temperature peaks are found, especially in stratified flow at higher void fractions. The transient behaviour of the absorber tube has been analysed by stepwise increasing or decreasing the solar irradiation. The response time of the absorber tube is between 70 and 140 s for different void fractions inside.

INTRODUCTION

IF WE LOOK at the various concepts of solar thermal power generation for processing steam and electricity, the solar farm concept using parabolic trough collectors shows the best economy of all. Since 1984 the Luz Engineering Corporation has built seven Solar Electric Generating Systems (SEGS) near Los Angeles with a total capacity of about 194 MW [1, 2]. A new plant called SEGS-8 with 80 MW is under construction. The electrical energy cost is predicted to be 8 cents per kWh.

The technical concept is given in principle. The collector field is built up of parabolic troughs orientated in the east–west direction and solar tracked in one axis. The solar irradiation is focused to the central absorber tube with a concentration factor between 60 and 80. In Fig. 1 a solar collector assembly is shown schematically. An evacuated glass tube around the absorber tube reduces heat losses. The heat transfer oil flowing through the absorber tube is heated from 293°C to 393°C. Steam at 100 bar and 370°C is produced in a conventional steam generator and drives a turbine and an electrical generator. The total efficiency is about 37.5%. Detailed technical information on such power plants is given in ref. [1].

In an earlier work [3] water at a pressure of about 90 bars, instead of heat transfer oil, was used. The pressurized water circulated through a field of solar collectors and was then brought to a boiler in order to produce steam in a second loop from the power station. The main advantage of this system was the avoidance of two-phase flow in the collection network, which can cause flow instabilities and difficulties during start-up and shutdown operations. On the other hand, its main disadvantage was the high mass flow rate in the pressurized water section. This requires extremely large and expensive pipes for the inlet and outlet lines of the pressurized water loop.

The advantages of direct steam generating in a solar collector instead of using a heat transfer oil were given in ref. [4]. Reduced flow rate and reduced operating temperatures in the collector field were named.

Thermal analysis of boiling refrigerant in a flat-plate solar collector is also found in the literature, e.g. ref. [5].

There are many advantages if only one loop is used with direct steam generation in the absorber tubes instead of a primary oil loop and a secondary water/steam loop.

The advantages of direct steam generation may be summarized as follows:

reduced amount of equipment;
reduced auxiliary energy for pumping;
no loss of exergy in the evaporator;
saving the cost of the expensive heat transfer oil;

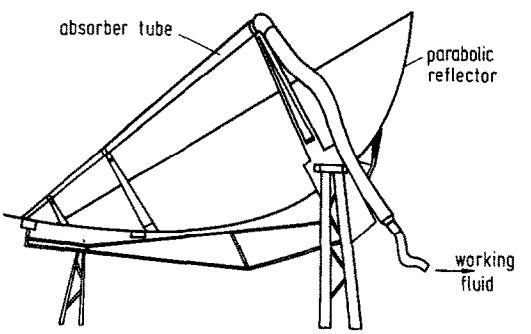

FIG. 1. Scheme of a parabolic trough collector.

† Dedicated to Professor Dr.-Ing. Dr.-Ing.e.h. Ulrich Grigull.

NOMENCLATURE

A, B, C^*, D	finite difference coefficients
c_p	specific heat capacity
C_{opt}	concentration factor
d	diameter
E_{glob}	solar irradiation
q	heat flux
q^*	heat generation rate
r	radius
t	time
x	quality.

Greek symbols

α^*	absorptivity
α_l	heat transfer coefficient, liquid phase
α_v	heat transfer coefficient, vapour phase
Δ	difference
ε	volumetric void fraction
ϑ	temperature
λ	thermal conductivity
ρ	density
σ	finite difference factor
φ	perimeter angle.

Subscripts

am	ambient
i, j	nodal point number
in	inner
k	time step
l	lower
o	outer
s	saturated
u	upper
v	vapour.

higher initial steam pressure and temperature and higher efficiency;

better time response in changing operational conditions;

high heat transfer coefficients during boiling.

Nevertheless, a number of problems and disadvantages can also be named:

two-phase flow with varying heat transfer at the inner circumference, low heat transfer coefficient in the vapour phase (upper tube surface) and high heat transfer coefficient in the liquid phase (lower tube surface);

possible deformation because of great differences in wall temperature in the axial and circumferential directions;

high pressures in long pipes of relatively large diameter (0.12 m);

two-phase flow instabilities and vapour blockage;

need of dynamic process control for changing solar irradiation;

need of a vapour storage to compensate fluctuation in irradiation and load distribution;

need of mass flow control.

In order to eliminate problems and uncertainties, experiments are required. These, however, are expensive and time-consuming since large test facilities are involved. Thus, such experiments should be preceded by detailed calculations. This is done here.

The problem of asymmetric heat transfer distribution at the inner tube wall during boiling in horizontal tubes has been discussed in the literature [6–8]. In all these cases constant heat flux over the total outer circumference has been considered. In this work, an asymmetric heat flux distribution at the outer tube wall will be studied.

THEORY

Mathematical model and boundary conditions

A typical cross-section of the absorber tube with boundary conditions is illustrated in Fig. 2. In order to calculate the temperature distribution within the tube wall under various conditions, the following set of general assumptions is made:

(i) the thermophysical properties λ, c_p and ρ of the tube material are constant;

(ii) the local heat transfer coefficients in the liquid and vapour phases of the two-phase flow inside the tube are uniform over the respective inner surface and only stratified flow is considered;

(iii) the local heat transfer coefficient at the outer tube wall is also uniform;

(iv) the ambient temperature is time independent;

(v) sun tracking of the concentrator is not taken into account.

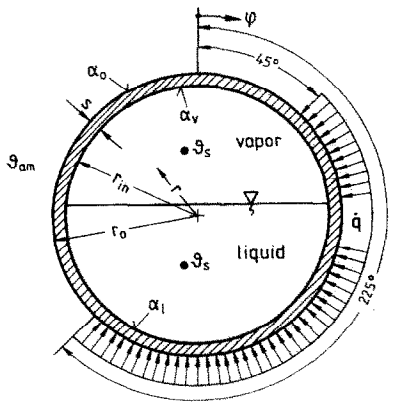

FIG. 2. Cross-section of the absorber tube with boundary conditions.

Table 1. Heat transfer coefficients in the liquid and vapour phases for various void fractions

x [—]	ε [—]	α_l (W m^{-2} K^{-1})	α_v (W m^{-2} K^{-1})
0.01	0.10	5000	500
0.10	0.55	7500	650
0.50	0.85	12 000	1800

Knowing the quality x of the two-phase flow inside the tube, the heat transfer coefficients in the liquid and vapour phases (α_l, α_v) can be calculated according to ref. [9]. Results are listed in Table 1. The void fraction ε is obtained from the quality x using a two-phase flow model.

The bulk temperature in both phases is assumed to be at a constant value of $\vartheta_s = 311°C$, which corresponds to the saturation temperature at $p_s = 100$ bar of the working fluid water.

The heat conduction equation in cylindrical coordinates is given as follows:

$$\frac{\partial \vartheta}{\partial t} = \frac{\lambda}{\rho \cdot c_p}\left[\frac{\partial^2 \vartheta}{\partial r^2} + \frac{1}{r}\cdot\frac{\partial \vartheta}{\partial r} + \frac{1}{r^2}\frac{\partial^2 \vartheta}{\partial \varphi^2}\right] + \frac{q^*}{\rho \cdot c_p}. \quad (1)$$

The boundary conditions of the outer tube wall are:

$$-\lambda \cdot \left.\frac{\partial \vartheta}{\partial r}\right|_{r_o} = [\vartheta(r_o) - \vartheta_{am}] \cdot \alpha_o \quad (1a)$$

at

$$0° < \varphi < 45° \quad \text{and} \quad 225° < \varphi < 360°$$

$$q = \alpha^* C_{opt} E_{glob} \quad \text{at} \quad 45° < \varphi < 225° \quad (1b)$$

where φ denotes the perimeter angle, α^* the absorptivity of the tube material, C_{opt} the concentration factor of the parabolic trough and E_{glob} the solar irradiation. A combined heat transfer coefficient α_o is applied to characterize heat transfer by long-wave thermal radiation and natural convection at the outside of the absorber tube. The boundary conditions at the inner tube wall are:

$$-\lambda \cdot \left.\frac{\partial \vartheta}{\partial r}\right|_{r_{in}} = [\vartheta(r_{in}) - \vartheta_s] \cdot \alpha_l \quad \text{in the liquid phase} \quad (1c)$$

$$-\lambda \cdot \left.\frac{\partial \vartheta}{\partial r}\right|_{r_{in}} = [\vartheta(r_{in}) - \vartheta_s] \cdot \alpha_v \quad \text{in the vapour phase.} \quad (1d)$$

The size of the wetted and unwetted area on the inner tube wall depends on the void fraction.

With equations (1)–(1d) the description of the temperature distribution inside the absorber wall is possible at different operating modes of the trough collector. The following cases are considered:

(a) *steady-state calculations*: by using $dt \to \infty$, time derivatives in equation (1) are negligible. The Laplace equation is obtained subject to boundary conditions (1a)–(1d), in which heat flux q is considered to be time independent (q = const.);

(b) *transient calculations*: therefore the heat flux q in the Neumann boundary condition (1b) is assumed to be dependent on time ($q = q(t)$). Initially a temperature distribution as calculated under steady-state condition (a) is used.

Finite difference solution

The solution of equation (1) by means of finite differences is well known [10, 11]. After discretization the solution vector ϑ of the resulting generalized system

$$[A]\,\vartheta = b \quad (2)$$

can be obtained by multiplying the inverse of the matrix $[A]$ with the so-called boundary vector b

$$\vartheta = [A]^{-1} b. \quad (3)$$

The coefficient matrix $[A]$ as well as the vector b depend on a set of parameters such as geometric dimensions, selected discretization scheme, transient or steady-state operation mode, heat transfer coefficients and material properties. If one or more of the listed parameters have to be changed, the matrix $[A]$ and the vector b have to be adapted to the new condition. This can be a lengthy and cumbersome procedure, especially when changing the discretization scheme.

Using the discretization scheme shown in Fig. 3, a modular nodal point library was developed and used to generate easily the generalized form of equation (2) for each parameter combination of the absorber tube with the boundary conditions. Therefore a general difference equation was used which can be written as

$$\begin{aligned}
&(\sigma-1)\cdot B_{l,i,j}\cdot \vartheta_{i-1,j,k+1} + (\sigma-1)\cdot A_{l,i,j}\cdot \vartheta_{i,j-1,k+1} \\
&\quad + \left[\frac{C^*_{i,j}}{\Delta t} - (\sigma-1)\cdot D_{i,j}\right]\cdot \vartheta_{j,i,k+1} + (\sigma-1)\cdot A_{u,i,j} \\
&\quad \cdot \vartheta_{i,j+1,k+1} + (\sigma-1)\cdot B_{u,i,j}\cdot \vartheta_{i+1,j,k+1} \\
&= \sigma \cdot B_{l,i,j}\cdot \vartheta_{i-1,j,k} + \sigma \cdot A_{l,i,j}\cdot \vartheta_{i,j-1,k} + \left[\frac{C^*_{i,j}}{\Delta t} - \sigma \cdot D_{i,j}\right] \\
&\quad \cdot \vartheta_{i,j,k} + \sigma \cdot A_{u,i,j}\cdot \vartheta_{i,j+1,k} + \sigma \cdot B_{u,i,j}\cdot \vartheta_{i+1,j,k} \\
&\quad + [\sigma \cdot q^*_k - (\sigma-1)\cdot q^*_{k+1}]\cdot \Delta\varphi_{i,j}\cdot \Delta r_{i,j}\cdot r_{i,j}
\end{aligned} \quad (4)$$

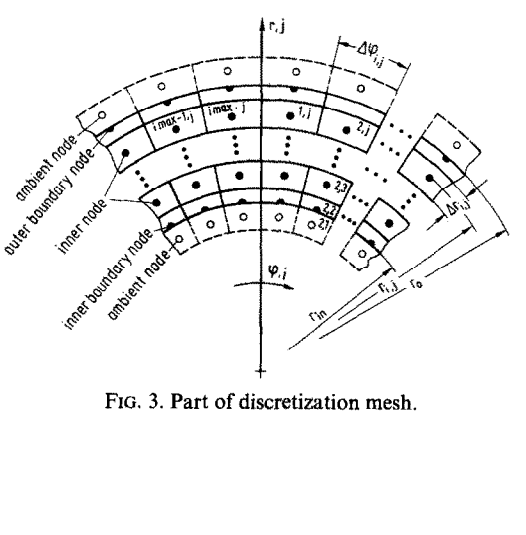

FIG. 3. Part of discretization mesh.

with

$$D_{i,j} = B_{l,i,j} + A_{l,i,j} + A_{u,i,j} + B_{u,i,j} \quad (4a)$$

and

$$C^*_{i,j} = c_{p,i,j} \cdot \rho_{i,j} \cdot \Delta\varphi_{i,j} \cdot \Delta r_{i,j} \cdot r_{i,j}. \quad (4b)$$

Time-dependent values at times t and $t+\Delta t$ are indicated with k and $k+1$. The finite difference coefficients A_l, A_u, B_l and B_u represent the heat transfer coefficient times the transfer area between neighbouring temperature nodes; they are dependent on the nodal location. The coefficients A_l, A_u, B_l, B_u and D are diagonal elements of the pentadiagonal matrix $[A]$ in equation (2). The right-hand-side of equation (4) represents an element of the boundary vector b. With special values for the finite difference factor σ and time-step Δt, various finite difference formulations are obtained as follows:

$\sigma = 0$, $\Delta t \to \infty$: steady-state pure implicit formulation;

$\sigma = 1$, Δt finite: transient pure implicit formulation;

$\sigma = 0.5$, Δt finite: transient Crank–Nicholson formulation.

Depending on their position inside the discretization mesh (see Fig. 3), inner and boundary nodes within the control volume can be distinguished. In order to describe the temperature of the surrounding ambient medium as a function of time and adiabatic boundary conditions, special massless nodes were used. For each type of temperature node within the control volume a Fortran subroutine was written which contains the calculation formulae for A_l, A_u, B_l, B_u and C^*. The summary of different nodes' Fortran routines, supplied with different index numbers, constitute the nodal point library.

Different boundary nodes, one inner and two special nodes, were used in a 9×360 mesh for the absorber tube simulations. Each volume element was assigned to a suitable nodal point index number. By interpreting the resulting index matrix using the nodal library, the unknown coefficients A_l, A_u, B_l, B_u and C^* were evaluated for each location inside the mesh. Then the matrix $[A]$ and the vector b were calculated for the given parameter combination with equation (4). The Neumann-type boundary condition (1b) was modelled by substituting $q/\Delta r_{i,j}$ for q^* in equation (4). The control volumes at locations ($i$max, j) and (1, j) were coupled by setting $\vartheta_{i\max,j} = \vartheta_{1,j}$. In the case of steady-state calculations, equation (2) was solved iteratively using a modified alternating direction implicit (ADI) procedure for elliptic problems as given in ref. [12]. Therefore with $\sigma = 1$, the term $2C^*_{i,j}/\Delta t$ in equation (4) has to be changed into $D_{i,j} \cdot K$. The factor K has to be adapted after each iteration. After rapid convergence the results showed some oscillations, so a follow-up iteration by an over-relaxation method was necessary.

Transient calculations using the iterative over-relaxation method showed a strong computation time dependency of the relaxation factor on the inner and outer heat transfer coefficients. In order to provide the empirical determination of the relaxation factor, all transient calculations were performed using the implicit ADI procedure. Compared to the relaxation method with the Crank–Nicholson finite difference formulation a decrease of the computation time of up to 90% was achieved. In order to provide numerically induced oscillations, a time-step adaption was used.

Table 2. Standard values used in calculations

Absorber tube	
Outer diameter d_o	127 mm (5″)
Wall thickness s	6 mm
Thermal conductivity λ	17 W m^{-1} K^{-1}
Density ρ	7500 kg m^{-3}
Specific heat capacity c_p	500 J kg^{-1} K^{-1}
Absorptivity α^*	0.833
Concentration factor C_{opt}	60
Ambient temperature ϑ_{am}	40°C
Fluid temperature ϑ_s	311°C
Heat transfer coefficient α_o (convection and radiation)	15 W m^{-2} K^{-1}

The standard values shown in Table 2 are used in the calculations.

RESULTS AND DISCUSSION

Steady-state operating conditions

The temperature fields in the absorber tube walls in Fig. 4 were calculated at a constant irradiation of 1000 W m^{-2}. If one takes into account the concentration factor $C_{opt} = 60$ and the absorptivity of the tube $\alpha^* = 0.833$, a heat flux of 50 000 W m^{-2} is obtained on the outer tube wall section which is irradiated from the trough. This section is marked in Fig. 4 by a segment of a concentric circle with arrows pointing to the absorber tube. The difference between two isotherms in Fig. 4 is 5 K.

The void fraction was varied in Fig. 4(a–c) keeping all other parameters fixed. In the region where the irradiation drops from the concentrated to only solar irradiation the isotherms are in the radial direction, i.e. heat is flowing within the tube wall to regions of lower temperature at the top and bottom of the tube. In the wetted region the isotherms are nearly concentric to the tube wall, i.e. heat flows radially on the shortest route from the outer tube wall to the boiling fluid. The highest temperatures occur on the outer tube wall in the non-wetted section irradiated from the trough.

At a low void fraction $\varepsilon = 0.1$ (Fig. 4(a)) the maximum temperature of about 335°C is rather constant on the outer tube perimeter which is irradiated from the trough. The lowest temperatures occur in the part of the tube that the sun irradiates directly. For $\varepsilon = 0.55$ the maximum temperature is about 390°C (Fig. 4(b)). For $\varepsilon = 0.85$ the temperature goes

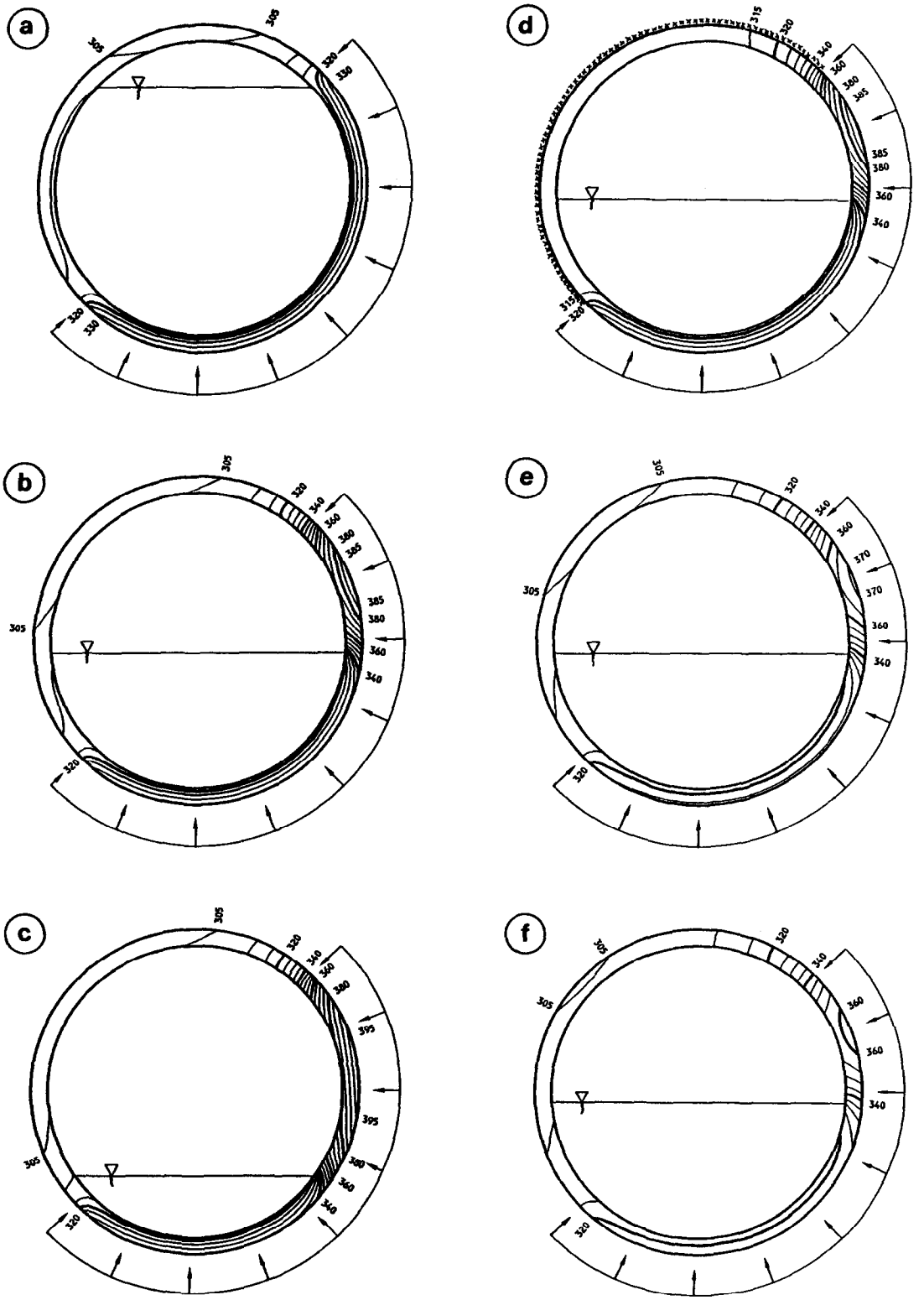

FIG. 4. Temperature fields under steady-state operating conditions: (a) $\varepsilon = 0.1$; (b) $\varepsilon = 0.55$; (c) $\varepsilon = 0.85$; (d) with thermal insulation; (e) $\lambda = 35\ \mathrm{W\ m^{-1}\ K^{-1}}$; (f) $\lambda = 52\ \mathrm{W\ m^{-1}\ K^{-1}}$.

up to 400°C (Fig. 4(c)). In all three cases regions with temperatures below 305°C are found at the inner wall. This is below the saturation temperature of 311°C, so that recondensation will occur. The areas with a temperature below the saturation temperature increase with increasing void fraction (compare Fig. 4(a–c)).

In general, the largest temperature gradients are observed at locations where the heat flow direction changes, i.e. where irradiation changes in the unwetted region and between unwetted and wetted regions in the section irradiated from the trough.

In order to reduce heat losses and recondensation a thermal insulation is applied to the tube section that is not irradiated from the trough (Fig. 4(d)). This case is simulated as an adiabatic boundary condition. The result is that the temperature of the inner tube wall does not fall below the saturation temperature. A comparison of Fig. 4(d) with Fig. 4(b) shows that the temperature in the section irradiated from the trough has not changed much. This can be explained by the relatively low thermal conductivity of the absorber tube.

The effect of higher thermal conductivities was studied so that high temperature gradients and high temperature differences in the absorber tube wall can be avoided. If the thermal conductivity is increased from 17 up to 35 W m^{-1} K^{-1} (Fig. 4(c)) the maximum temperature decreases from 390°C to 372°C. If the thermal conductivity is 52 W m^{-1} K^{-1} (Fig. 4(f)), the maximum temperature becomes only 365°C. In both cases with higher thermal conductivity, however, inner wall regions with temperatures below saturation temperature do occur. The problem of recondensation therefore still remains if no thermal insulation is used.

Table 3. Measured data (Almeria) for solar irradiation as a function of time

Time (min)	0	30	60	90	120	150	180	210
E_{glob} (W m^{-2})	500	639	717	757	784	808	827	834

Transient operating conditions

Transient operating conditions will be experienced if solar radiation in equation (1b) is a function of time. Two different cases are considered.

(1) The solar radiation is a function of daytime only.

(2) The solar radiation is subject to sudden changes, e.g. shading. Shading effects are modelled by assuming a step change of the solar radiation from 1000 W m^{-2} to zero.

According to the assumption of a steady-state boiling process inside the tube, transient calculations are only meaningful as long as the calculated temperatures at the wetted part of the inner tube wall are higher than the saturation temperature. Therefore in the case of increasing solar irradiation (case 1), initially a temperature distribution as calculated for E_{glob} = 500 W m^{-2} was used. For suddenly decreasing irradiation (case 2), the calculations were stopped if the saturation temperature was reached at the wetted part of the inner tube wall. Additionally it was assumed that changes in irradiation do not affect the void fraction. That means that the mass flow rate of the working fluid has to be adapted.

Simulation of a daily sun course. Based on discrete values from Almeria, Spain (Table 3), a functional

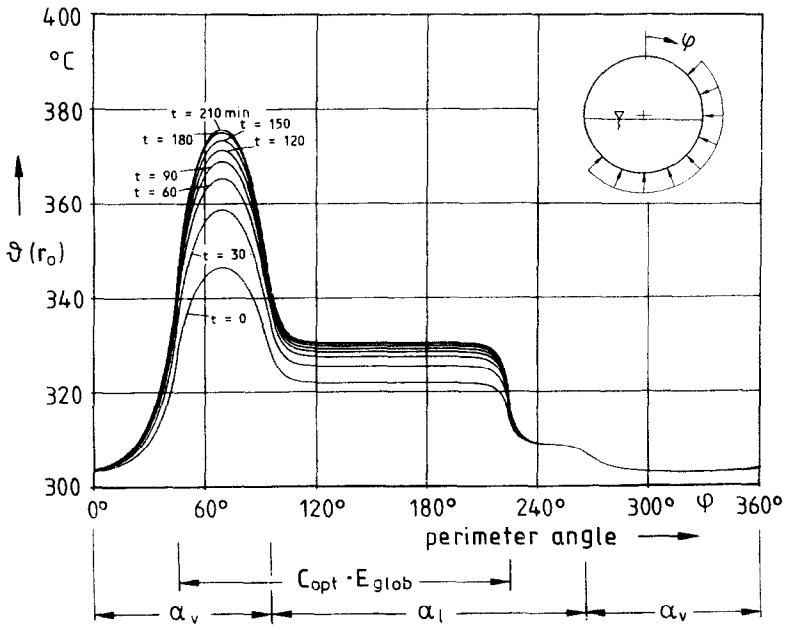

FIG. 5. Temperature profile at the outer tube wall during a daily sun course (ε = 0.55).

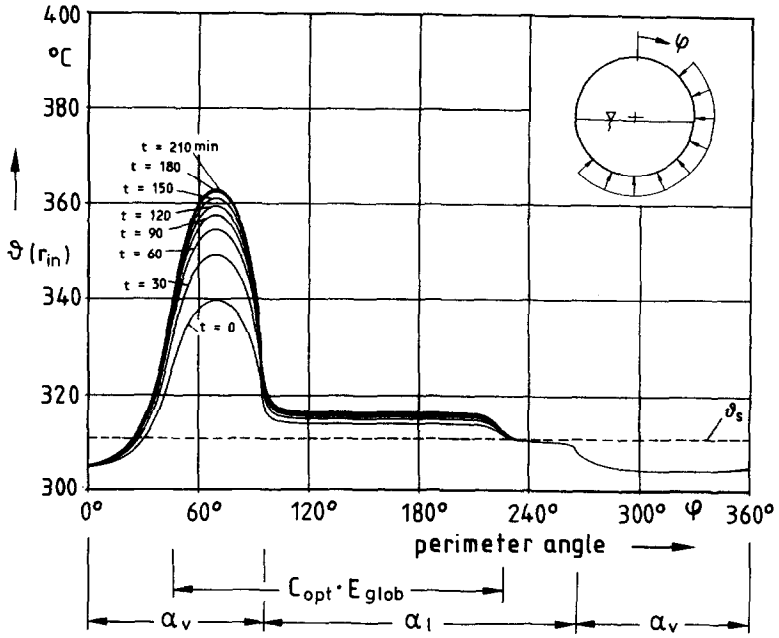

FIG. 6. Temperature profile at the inner tube wall during a daily sun course ($\varepsilon = 0.55$).

approach for the time dependence of the solar irradiation was evaluated by means of polynomial regression. Only E_{glob} values larger than 500 W m^{-2} (reached at about 9 a.m.) up to a maximum irradiation of 834 W m^{-2} were used. With this excitation (Table 3), temperature distributions as shown in Figs. 5 and 6 are calculated.

Figure 5 shows the temperature of the outer surface of the absorber tube vs perimeter angle for various times ($\varepsilon = 0.55$). Figure 6 shows the temperature of the inner surface. It is seen in both figures that a rapid temperature change only occurs in the unwetted tube region in the range $45° < \varphi < 90°$. In the wetted region ($90° < \varphi < 220°$) the temperature increase is about 10 K at the outer tube wall and 5 K at the inner wall. In the remaining tube region ($220° < \varphi < 360°$

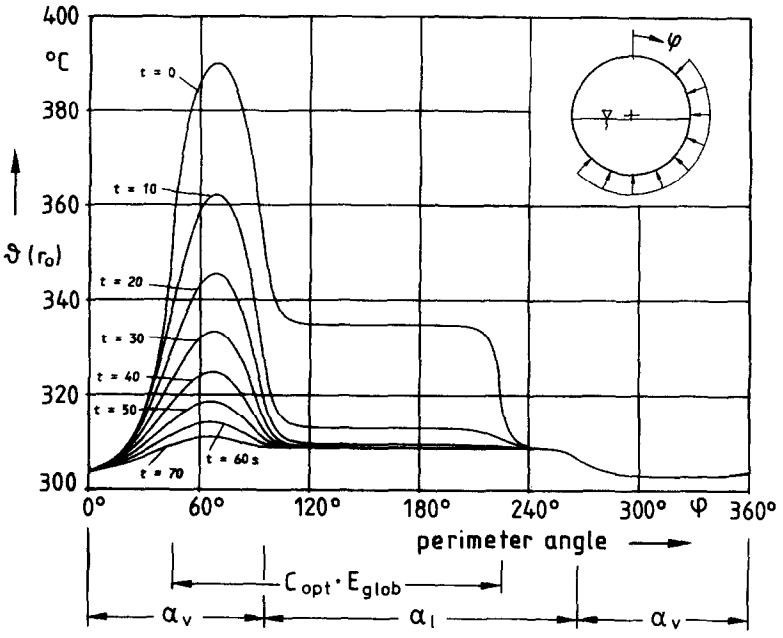

FIG. 7. Temperature profile at the outer tube wall at sudden shadowing ($\varepsilon = 0.55$).

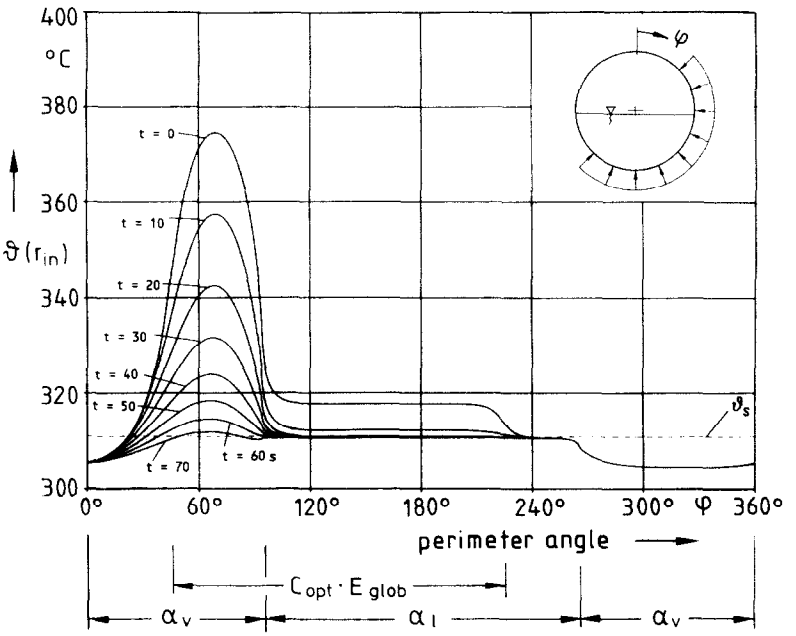

FIG. 8. Temperature profile at the inner tube wall at sudden shadowing ($\varepsilon = 0.55$).

and $0° < \varphi < 45°$) the wall temperature is found to be time independent. The calculations show that the local temperature gradient at the boundary between liquid and vapour phases ($\varphi = 90°$) is much greater at the inside than at the outside of the tube.

Simulation of shadowing effects. The inner and outer wall temperatures vs the perimeter angle φ are shown in Figs. 7 and 8 as functions of time for a sudden drop of irradiation. At time zero a temperature distribution as calculated for $E_{glob} = 1000$ W m^{-2} was assumed. After setting the solar irradiation equal to zero the boiling process inside the tube is still going on as it is maintained by the heat which is stored in the tube wall. The calculations showed that, within the boiling zone ($100° < \varphi < 220°$), the outer wall temperature is below the inner wall temperature after 15 s. In this case the heat flow direction is from the inside to the outside of the tube. The inner wall temperature reaches saturation temperature ϑ_s after 20 s and therefore the boiling process will stop. The thermal behaviour of the system depends on the response time of the absorber tube. This was calculated for given void fraction $\varepsilon = 0.55$ at 140 s and for $\varepsilon = 0.85$ at 70 s. A small response time is advantageous with respect to the start-up behaviour of the entire system but disadvantageous considering the stability under sudden shadowing.

CONCLUSIONS

In order to reduce high temperature gradients and temperature differences inside the absorber tube wall a tube material with higher thermal conductivity appears appropriate. The tube deformation due to asymmetric thermal expansion can then be minimized. The reflected irradiation from the parabolic trough should be directed onto the part of the tube that is wetted inside. This could be achieved by adjusting the troughs depending not only on the sun position but also on the two-phase flow pattern inside.

The transient calculations show the necessity of steam storage in solar farm power plants in order to balance not only longer periods without irradiation but also short time shading effects. In the case of a sudden drop of irradiation, very high temperature gradients inside the absorber tube can be induced within a short time.

REFERENCES

1. M. Geyer and H. Klaiß, 194 MW Solarstrom aus Rinnenkollektoren, *Brennstoff-Wärme-Kraft* **41**(6), 288–295 (1989).
2. D. Jaffe, S. Friedlander and D. Kearney, The Luz solar electric generating systems in California, *Proc. Biennial Congress of the International Solar Energy Society*, Hamburg, Germany, Vol. 1, pp. 519–529 (1987).
3. J. W. Ramsey, E. M. Sparrow and E. R. G. Eckert, Solar-thermal electric power generation using a system of distributed parabolic trough collectors, *A.I.Ch.E. Symp. Ser.* **74**(174), 271–280 (1978).
4. J. W. Allen and W. M. Schertz, Steam-generating collectors, Argonne National Laboratory, Argonne, IL, CONF-830874-26, DE 83017938 (1983).
5. A. Y. El-Assy, Thermal analysis and operational limits of compound parabolic concentrators in two-phase flows with saturated exit states, *Wärme- und Stoffübertragung* **23**, 167–173 (1988).
6. R. Dolezal, Rohrkühlung bei der Schichtströmung im

waagrechten Siederohr eines Abhitzekessels, *Brennstoff-Wärme-Kraft* **43**(7/8), 364–367 (1991).
7. W. Bonn, J. Iwicki, R. Krebs, D. Steiner and E. U. Schlünder, Über die Auswirkung der Ungleichverteilung des Wärmeübergangs am Rohrumfang bei der Verdampfung im durchströmten waagrechten Rohr, *Wärme- und Stoffübertragung* **13**, 265–274 (1980).
8. H. Schmidt and D. Steiner, Einfluß der Beheizungsart auf den Wärmeübergang im horizontalen Verdampferrohr, *Wärme- und Stoffübertragung* **24**, 289–301 (1989).
9. D. Steiner, *Wärmeübertragung beim Sieden gesättigter Flüssigkeiten*, Kap. Hbb, VDI Wärmeatlas, 5. Auflage. VDI-Verlag, Düsseldorf (1988).
10. R. C. Croft and D. G. Lilley, *Heat Transfer Calculations Using Finite Difference Equations*. Applied Science Publishers, London (1977).
11. H. Köhne, Digitale und analoge Lösungsmethoden der Wärmeleitungsgleichung, *Forschungsbericht des Landes Nordrhein-Westfalen* No. 2120 (1970).
12. D. Marsal, *Die numerische Lösung partieller Differentialgleichungen in Wissenschaft und Technik*. Bibliographisches Institut Mannheim, Zürich (1976).

CHAMP DE TEMPERATURE PERMANENT OU VARIABLE DANS UN TUBE ABSORBEUR D'UN COLLECTEUR SOLAIRE DE GENERATEUR DE VAPEUR

Résumé—On calcule le champ de température dans un tube absorbeur de collecteur parabolique de générateur de vapeur. On considère les conditions de fonctionnement permanentes et variables. Un programme universel est développé pour résoudre le champ de température bidimensionnel en utilisant une librairie modulaire à point nodal. Le champ de température est extrêmement asymétrique à cause de la variation du coefficient de transfert à la surface interne et à l'irradiation solaire à la surface extérieure du tube absorbeur. On constate des pics élevés de température, spécialement dans le cas de l'écoulement stratifié, pour des grandes fractions de vide. Le comportement variable du tube absorbeur a été analysé par pas pour une irridation solaire croissante ou décroissante. Le temps de réponse du tube absorbeur est entre 70 et 140 s pour différentes fractions de vide interne.

STATIONÄRE UND INSTATIONÄRE TEMPERATURFELDER IM ABSORBERROHR EINES KONZENTRIERENDEN SONNENKOLLEKTORS MIT DIREKTVERDAMPFUNG

Zusammenfassung—Es wird das Temperaturfeld im Absorberrohr eines Parabolrinnenkollektors mit Direktverdampfung von Wasser berechnet. Stationäre und instationäre Betriebszustände werden betrachtet. Zur Berechnung des zweidimensionalen instationären Temperaturfeldes wird ein universelles Computerprogramm mit einer modularen Knotenbibliothek entwickelt. Auf Grund der ungleichförmigen Verteilung des Wärmeübergangskoeffizienten auf der Innenseite und der Wärmestromdichte auf der Aussenseite des Absorberrohres ergeben sich extrem asymmetrische Temperaturverteilungen. Besonders bei der Schichtenströmung mit hohem Dampfgehalt stellt man große Temperaturspitzen fest. Das instationäre Verhalten des Absorberrohres wird durch Simulation einer plötzlichen Abschattung und eines Tagesganges ermittelt. Die Zeitkonstante des Absorberrohres liegt zwischen 70 und 140 s je nach Dampfgehalt der Strömung.

СТАЦИОНАРНОЕ И НЕСТАЦИОНАРНОЕ ТЕМПЕРАТУРНОЕ ПОЛЕ В ТРУБЕ АБСОРБЕРА ПРЯМОГО ПАРОГЕНЕРАТОРНОГО СОЛНЕЧНОГО КОЛЛЕКТОРА

Аннотация—Рассчитывается температурное поле трубы абсорбера прямого парогенераторного параболического коллектора. Рассматриваются стационарные и нестационарные режимные параметры. Разработана универсальная программа для решения задачи о двумерном нестационарном поле температур с использованием библиотеки модулярных узловых точек. Вследствие изменения коэффициента теплопередачи на внутренней поверхности трубы абсорбера и солнечной радиации на внешней поверхности температурное поле является крайне асимметричным. Обнаружены заметные температурные пики, особенно для условий стратифицированного течения при высоких значениях истинного паросодержания. Переходные характеристики трубы абсорбера определялись посредством скачкообразного увеличения или уменьшения солнечной радиации. Время отклика трубы абсорбера изменяется в интервале 70–140 секунд при различных значениях истинного паросодержания.